Role of Aspartate 94 in the Decay of the Peroxide Intermediate in the Multicopper Oxidase Fet3p†

Liliana Quintanar,‡ Christopher Stoj,§ Tzu-Pin Wang,§ Daniel J. Kosman,*,§ and Edward I. Solomon*,‡

Department of Chemistry, Stanford University, Stanford, California 94305-5080, and Department of Biochemistry, School of Medicine and Biomedical Sciences, State University of New York, Buffalo, New York 14214

Received December 13, 2004; Revised Manuscript Received March 7, 2005

ABSTRACT: Fet3p is a multicopper oxidase that contains four Cu ions: one type 1, one type 2, and a coupled binuclear type 3 site. The type 2 and type 3 centers form a trinuclear cluster that is the active site for O_2 reduction to H_2O. When the type 1 Cu is depleted (C484S mutation), the reaction of the reduced trinuclear cluster with O_2 generates a peroxide intermediate. Kinetic studies of the decay of the peroxide intermediate suggest that a carboxyl residue (D94 in Fet3p) assists the reductive cleavage of the O−O bond at low pH. Mutations at the D94 residue (D94A, D94N, and D94E) have been studied to evaluate its role in the decay of the peroxide intermediate. Spectroscopic studies show that the D94 mutations affect the geometric and electronic structure of the trinuclear cluster in a way that is consistent with the hydrogen bond connectivity of D94. While the D94E mutation does not affect the initial reaction of the cluster with O_2, the D94A mutation causes larger structural changes that render the trinuclear cluster unreactive toward O_2, demonstrating a structural role for the D94 residue. The decay of the peroxide intermediate is markedly affected by the D94E mutation, confirming the involvement of D94 in this reaction. The D94 residue appears to activate a proton of the type 2 Cu^+-bound water for participation in the transition state. These studies provide new insight into the role of D94 and proton involvement in the reductive cleavage of the O−O bond.

The multicopper oxidases are an important class of enzymes present in bacteria, fungi, plants, and animals that couple the four-electron reduction of O_2 to H_2O with the one-electron oxidation of four substrate equivalents (*1*). Ascorbate oxidase (AO),[1] human ceruloplasmin, Fet3p, and laccases are among the most studied members of this family. Fet3p is a plasma membrane protein in *Saccharomyces cerevisiae* (*2*−*4*) that, along with the iron permease Ftr1p, plays an integral role in high-affinity iron uptake in yeast (*5*, *6*).

The catalytic motif in all multicopper oxidases includes at least one type 1 (T1) or blue Cu, one type 2 (T2) or normal Cu, and one type 3 (T3) or coupled binuclear Cu site (*1*). The T1 Cu site is characterized by an intense Cys → Cu charge transfer (CT) transition at ∼600 nm and small (<100 × 10^{-4} cm^{-1}) parallel hyperfine coupling in electron paramagnetic resonance (EPR). The T2 Cu site has no distinctive absorption features and a large parallel hyperfine coupling (∼200 × 10^{-4} cm^{-1}) by EPR. A detailed spectroscopic investigation of laccase has shown that there is a water-derived ligand at the T2 Cu which remains hydroxide over the pH range of 4.7−10 (*7*). The T3 site is comprised of two Cu ions that are antiferromagnetically coupled through a bridging hydroxide. Thus, the T3 site is diamagnetic and shows no EPR signal, but it exhibits a CT transition at ∼330 nm in the absorption spectrum. The T2 and T3 sites form a trinuclear Cu cluster, which is the site of dioxygen binding and reduction (*8*−*11*), while the main functional role of the T1 Cu site is to shuttle electrons from the substrate to the trinuclear Cu site (∼13 Å away).

Studies on the catalytic cycle of the multicopper oxidases have shown that the reduction of O_2 to water by the trinuclear cluster involves two $2e^-$ steps (*12*). Reaction of the fully reduced protein with O_2 produces a transient species, referred to as the native intermediate, which in turn decays into the resting oxidized enzyme (*13*, *14*). Spectroscopic studies on this intermediate reveal that it is a fully oxidized species (i.e., four electrons have been transferred to dioxygen), where all of the coppers of the trinuclear site are bridged by the fully reduced oxygen product (oxo or hydroxo) (*15*). Oxygen reactivity studies of the reduced trinuclear Cu cluster in protein derivatives that lack a T1 Cu site [as in T1-mercury-substituted (T1Hg) laccase (*16*, *17*) or in T1-depleted (T1D, C484S) Fet3p (*18*)] have identified an intermediate, in which the T2 Cu is reduced and the T3 Cu atoms are oxidized. Thus, two electrons have been transferred to dioxygen, and the trinuclear Cu site is bridged by peroxide. Spectroscopic studies have developed two possible structural models for the peroxide intermediate, both with peroxide bridging the T2 and T3 Cu sites, either in a $\mu_3(\eta^1)_3$ bridging mode or

† This research was supported by NIH Grants DK31450 (to E.I.S.) and DK53820 (to D.J.K.).

* To whom correspondence should be addressed. E.I.S.: phone, (650) 723-9104; fax, (650) 725-0259; e-mail, edward.solomon@stanford.edu. D.J.K.: phone, (716) 829-2842; e-mail, camkos@buffalo.edu.

‡ Stanford University.

§ State University of New York.

[1] Abbreviations: AO, ascorbate oxidase; T1, type 1; T2, type 2; T3, type 3; EPR, electron paramagnetic resonance; T1D, type 1 depleted; T1Hg laccase, type 1 mercury-substituted laccase; CD, circular dichroism; MCD, magnetic circular dichroism; LF, ligand field; CT, charge transfer.

10.1021/bi047379c CCC: $30.25
Published on Web 03/31/2005

Table 1: Partial Sequence Alignment of Multicopper Oxidases[a] Showing the Highly Conserved Asp Residue[b]

		T2			T3B													
CpAO	58-74	V	I	**H**	W	**H**	G	I	L	Q	R	G	T	P	W	A	**D**	G
RvLc	57-73	T	I	**H**	W	**H**	G	V	K	Q	P	R	N	P	W	S	**D**	G
CcLc	62-78	S	I	**H**	W	**H**	G	L	F	Q	R	G	T	N	W	A	**D**	G
TvLc	62-78	S	I	**H**	W	**H**	G	F	F	Q	A	G	T	N	W	A	**D**	G
Fet3p	79-95	S	M	**H**	F	**H**	G	L	F	Q	N	G	T	A	S	M	**D**	G

[a] Abbreviations: CpAO, *Cucurbita pepo medullosa* ascorbate oxidase (*20*); RvLc, *R. vernicifera* laccase (*21*); CcLc, *Coprinus cinereus* laccase (*22*); TvLc, *T. versicolor* laccase (*23*); Fet3p, *S. cerevisiae* Fet3p (*24*). [b] One out of all fungal laccases characterized thus far (*25*), *Trametes villosa 2* (*26*), has a glutamate instead of an aspartate in this position.

possibly as a μ-1,1-hydroperoxide (*16*, *19*). It has been shown that the peroxide intermediate is kinetically competent to be a precursor to the native intermediate and thus in the catalytic cycle of the multicopper oxidases.

A combination of kinetic and spectroscopic studies have revealed that the peroxide intermediate decays via electron transfer from the T2 Cu with cleavage of the O−O bond (*16*, *17*). The reductive cleavage of the O−O bond is pH dependent with a pK_a of 5.0 in Fet3p (pK_a 5.8 in laccase). The rate enhancement at low pH has been associated with the conjugate acid form of a nearby carboxylic residue that assists in the reductive cleavage of the O−O bond (*17*, *18*). The nearest acidic residue in the vicinity of the trinuclear cluster is D94 in Fet3p (D72 in laccase), which is highly conserved in all multicopper oxidases (Table 1). Therefore, we have proposed that D94 assists in the decay of the peroxide intermediate at low pH in Fet3p.

In this study, we have studied three mutations at the D94 residue (D94E, D94A, and D94N) to evaluate its role in the decay of the peroxide intermediate. D94A and D94N are found to be unreactive toward O_2. Detailed spectroscopic studies of the T1DD94E and T1DD94A proteins have been pursued[2] to assess and compare the effects of these D94 mutations on the geometric and electronic structure of the trinuclear Cu cluster. The kinetics of formation and decay of the peroxide intermediate in the T1DD94E mutant have also been examined and compared to those of T1D Fet3p. These studies provide new insight into the role of the D94 residue and the involvement of a proton in assisting the reductive cleavage of the O−O bond.

EXPERIMENTAL PROCEDURES

All chemicals were of reagent grade and used without further purification. Water was purified to a resistivity of 15−17 MΩ cm^{-1} using a Barnstead Nanopure deionizing system. Mutant *FET3* alleles were constructed directly in plasmid pDY148 by site-directed mutagenesis using the QuickChange kit from Stratagene. Complementary primers encoding the following mutations were used in PCR amplification of the vector: D94A, D94N, and D94E. In addition, appropriate primers were used in two sequential rounds of mutagenesis to produce the T1DD94A and T1DD94E double mutants. Following amplification of the mutant-encoding vectors in bacteria, the *FET3* sequences were confirmed by the Roswell Park Cancer Institute DNA Sequencing Laboratory. The mutant vectors were transformed into the DY3260AFT^{1up} yeast strain for soluble protein expression. Expression, isolation, and purification of soluble wt, D94A, D94N, D94E, T1DD94A, and T1DD94E Fet3 proteins were performed as previously described (*4*, *27*). Fet3p protein concentrations were determined by the standard dye-binding Bradford assay (*28*). Copper content was determined spectrophotometrically using 2,2′-biquinoline (*29*) or by flameless atomic absorption spectroscopy. The concentration of paramagnetic copper was determined from spin quantitation of EPR spectra using a 1.0 mM $CuSO_4 \cdot 5H_2O$ solution with 2 mM HCl and 2 M $NaClO_4$ standard (*30*).

Room temperature UV−visible absorption spectra were recorded using a Hewlett-Packard HP8452A or an Agilent 8453 diode array spectrophotometer. EPR spectra were obtained using a Bruker EMX spectrometer, ER 041 XG microwave bridge, and ER 4102ST cavity. All X-band samples were run at 77 K in a liquid nitrogen finger dewar. Q-band spectra were obtained at 77 K using an ER 051 QR microwave bridge, ER 5106QT resonator, and an Oxford continuous flow CF935 cryostat. EPR spectra were baseline-corrected and simulated using XSophe (Bruker). Room temperature circular dichroism (CD) and low temperature (5 K) magnetic circular dichroism (MCD) spectra in the UV−visible region were collected with a Jasco J-810-150S spectropolarimeter operating with an S-20 photomultiplier tube and an Oxford SM4000-8T magnet. CD and MCD spectra in the near-IR region were obtained with a Jasco J-200-D spectropolarimeter using a liquid nitrogen cooled InSb detector and an Oxford SM4000-7T magnet. CD samples were run in a 0.5 cm quartz cuvette. MCD samples were run in cells fitted with quartz disks and a 3 mm rubber spacer. All MCD spectra presented are the subtracted average of the +7T and −7T scans, [7 − (−7)]/2T, to eliminate glass-induced baseline shifts and to increase signal-to-noise ratios. Gaussian fitting of the CD and MCD spectra was performed using PeakFit 4.0 (Jandel). Stopped-flow absorption kinetics with ∼2 ms dead time were obtained using an Applied Photophysics SX.18MV stopped-flow absorption spectrophotometer equipped with a Hg/Xe arc lamp and outfitted with PEEK tubing. The tubing, plungers, and valves of the stopped-flow instrument were made anaerobic by washing with dithionite solution followed by several washes with degassed buffer. O_2 inclusion was prevented by a stream of N_2 gas through the system. The cell path length was 1 cm. The temperature was maintained using a water/ethanol temperature bath (Fisher Scientific Isotemp 3016).

All oxidized Fet3p samples for spectroscopic characterization were prepared in either 100 mM deuterated potassium phosphate buffer (for pDs between 6 and 8), 100 mM deuterated MES buffer (for pDs between 4.7 and 6), or 50 mM potassium phthalate buffer (for pDs below 5). Mixtures of 50% (v/v) buffer/glycerol-d_3 were used to obtain optical-quality glasses upon freezing. Final protein concentrations

[2] Holo D94A protein does not react with O_2 (section 4). This is also found to be the case for D94N. Given the similar behavior of the D94A and D94N mutants, detailed spectroscopic and reactivity studies of the T1D forms have only been pursued on the T1DD94A protein.

Table 2: Characterization of Oxidized Fet3p Mutants

	Cu content (Cu/protein)	EPR spin quantitation (spin/protein)
wild type	4.2	1.8
D94A	3.9	1.5
D94N	3.8	1.6
D94E	4.3	1.8
T1D	3.2	0.8
T1DD94A	3.3	0.9
T1DD94E	3.2	0.7

were 0.3−0.8 mM. Addition of glycerol had no effect on the Cu sites, as assessed by EPR and absorption spectra.

Protein solutions for oxygen reactivity studies were prepared as described previously (*17*, *18*). Briefly, this involves reduction of the degassed protein by excess sodium dithionite inside a Vacuum Atmospheres Nexus-1 anaerobic globebox and removal of the excess dithionite by washing the protein solution with deoxygenated buffer, using a microcon concentration device (10000 MW cutoff, Amicon, Inc.). For fast measurements (formation of intermediates), the reduced and washed protein was loaded into the gastight syringe of an Applied Photophysics SX.18MV stopped-flow absorption spectrophotometer. The reduced protein was mixed with air-saturated buffer, and the reactions were followed at 20 °C; final protein concentrations were 15−20 μM, and the final O_2 concentration was 0.1 mM. For intermediate decay studies, the reduced protein was transferred into a 1 cm path length cuvette and mixed with O_2-saturated buffer; the reactions were followed using an HP8452A or an Agilent 8453 spectrophotometer at room temperature. Final protein concentrations were 40−50 μM, and the final O_2 concentration was 0.5 mM. All kinetic experiments were performed in either 100 mM phosphate buffer (for pHs between 6.5 and 8) or 100 mM MES buffer (for pHs between 4.7 and 6.5). When both buffers were employed at the same pH (6.5), there was no difference in the observed reaction rates.

RESULTS AND ANALYSIS

The following mutations were generated in Fet3p: D94A, D94N, D94E, T1DD94A, and T1DD94E. All holo proteins purify with ~4 Cu/protein, while all T1-depleted forms purify with ~3 Cu/protein (Table 2). Some mutants are mostly reduced in their as-isolated state; therefore, all proteins were treated with H_2O_2 (×4 equiv; excess H_2O_2 was removed by buffer exchanging into phosphate buffer, pD 7.5) prior to their spectroscopic characterization. Figure S1 (Supporting Information) shows the oxidation of the holo proteins, followed by absorption and EPR. The spin quantitation of the EPR spectra shows that the oxidized holo proteins contain ~2 spins/protein, and the T1-depleted forms contain ~1 spin/protein (Table 2).

(1) Spectroscopic Characterization of Holo Mutants. The absorption spectrum of Fet3p wild type (wt) is dominated by two envelopes of intense charge transfer (CT) bands: a band centered at 608 nm with $\epsilon = 5500\ M^{-1}\ cm^{-1}$ (associated with the T1 site) and a shoulder at 330 nm with an apparent $\epsilon = 5000\ M^{-1}\ cm^{-1}$ (associated with the T3 site; Figure S2A, Supporting Information)[3] (*31*). The D94A, D94N, and D94E Fet3 proteins exhibit the same CT bands with comparable extinction coefficients. Similarly, their CD (Figure S2B) and MCD (Figure S2C) spectra show no significant difference in the spectroscopic features of the T1 Cu site. The EPR spectrum of wt (Figure S3) shows signals from the T1 and T2 Cu sites, both with $g_{||} > g_{\perp} > 2.00$, indicative of $d_{x^2-y^2}$ ground states. The EPR spectra of the mutated proteins (Figure S3) show comparable T1 Cu EPR signals with a small parallel hyperfine splitting of $A_{||} = |88| \times 10^{-4}\ cm^{-1}$, as previously reported for Fet3p wt (*31*, *32*).

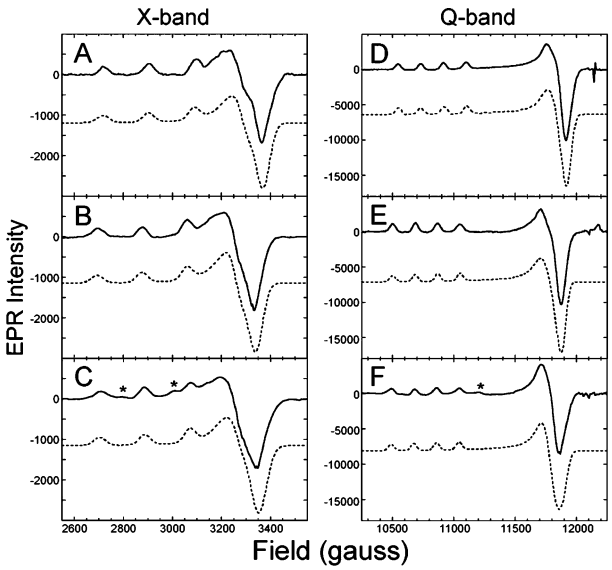

FIGURE 1: X-band EPR spectra of Fet3p T1D (A), T1DD94E (B), and T1DD94A (C) and Q-band EPR spectra of Fet3p T1D (D), T1DD94E (E), and T1DD94A (F). The presence of a second species in the T1DD94A EPR spectra is indicated with asterisks.[4] Experimental data (solid lines) and simulated spectra obtained with the parameters listed in Table 3 (dotted lines) are shown. X-band spectra were obtained at ~9.4 GHz microwave frequency, 10 mW microwave power, 100 kHz modulation frequency, 20 G modulation amplitude, 327 ms time constant, and 81.92 ms conversion time. Q-band spectra were obtained at ~34 GHz microwave frequency, 0.3 mW microwave power, 100 kHz modulation frequency, 10 G modulation amplitude, 327 ms time constant, and 163 ms conversion time. All spectra were collected at 77 K.

(2) Effects of the D94 Mutations on the Trinuclear Cluster in T1D Fet3p. (2.1) The T2 Site. Since the T1 Cu site dominates the spectra of the holo proteins, the spectroscopic perturbations of the trinuclear cluster caused by the D94 mutations are best studied in the T1D mutants.[2] The T3 site is diamagnetic; therefore, EPR and MCD spectra of the T1D forms show contributions only from the paramagnetic T2 site. The X-band (~9.4 GHz) and Q-band (~34 GHz) EPR spectra of T1D, T1DD94E, and T1DD94A are shown in Figure 1. For each mutant, X- and Q-band spectra were simultaneously simulated to obtain the ground-state spin Hamiltonian parameters listed in Table 3. Overall, the EPR spectra of T1DD94E (Figure 1B,E) and T1DD94A[4] (Figure 1C,F) are similar to those of T1D (Figure 1A,D), yet the

[3] The apparent extinction coefficient for the shoulder at 330 nm is 5000 $M^{-1}\ cm^{-1}$. However, once the spectrum of the reduced protein is subtracted (Figure 3), it lowers to about 3000 $M^{-1}\ cm^{-1}$. This is because the tail of the protein absorption at 280 nm contributes significantly at 330 nm.

[4] The presence of a second species is evident in the T1DD94A EPR spectra, as indicated with asterisks in Figure 1C,F. This is partially eliminated by chelating resin, increases at low pH, is not reversible with pH, and does not bind fluoride, indicating that it is an irreversibly denatured species.

Table 3: Spin Hamiltonian EPR Parameters for the T2 Cu Site

	T1D	T1DD94E	T1DD94A
g_x	2.041	2.038	2.039
g_y	2.055	2.055	2.055
g_z	2.243	2.243	2.245
A_x	15−20[a]	15−20[a]	20−25[b]
A_y	10−20[a]	10−20[a]	10−15[b]
A_z	190 ± 2	188 ± 2	189 ± 2

[a] For the EPR simulations shown in Figure 1, $A_x = 17$ and $A_y = 15$. [b] For simulations shown, $A_x = 25$ and $A_y = 15$. All hyperfine coupling constants are reported in $X \times 10^{-4}$ cm^{-1}.

Table 4: Gaussian Fits of Absorption, CD and MCD Spectra

MCD: T2 site

	T1D	T1DD94E	T1DD94A
band no.	energy	energy	energy
1 *xy*	(+) 9800	(+) 10000	(+) 10100
2 z^2	(−) 10540	(−) 11080	(−) 11600
3 *xz*	(+) 11700	(+) 11540	(+) 11200
4 *yz*	(−) 13940	(−) 14380	(−) 14100
5 His π	(−) 16700	(−) 16800	(−) 17130
6 OH π	(−) 20140	(−) 20400	(−) 20400
7 His π	(−) 24800	(−) 25280	(−) 25900
8 His π	(+) 28270	(+) 28300	(+) 28800
9 His π	(+) 30800	(+) 30900	(+) 30940

Abs/CD: T3 site

	T1D		T1DD94E		T1DD94A	
band no.	energy[a]	$\Delta\epsilon/\epsilon$[b]	energy[a]	$\Delta\epsilon/\epsilon$[b]	energy[a]	$\Delta\epsilon/\epsilon$[b]
1 d−d	10200	N/D	10200	N/D	9950	N/D
2 d−d	12500	−8.41	12430	−18.4	12280	−11.7
3 d−d	14080	1.39	15490	3.46	14750	2.41
4 d−d	15120	−9.47	13190	−0.99	13050	−2.68
5 d−d	17300	18.9	17200	23.1	18230	13.5
6 d−d	19630	31.2	19100	29.7	19970	27.3
7 His π	24770	−0.68	23900	−1.11	25600	−0.26
8 μ-OH	28000	0.38	28250	0.22	28200	0.22
9 μ-OH	30400	−0.18	30800	−0.17	30300	−0.082

[a] The energy of the transitions is reported in cm^{-1}. The energy was obtained from simultaneously fitting the CD and the difference absorption spectrum. The difference absorption spectrum (oxidized minus reduced spectrum) was used in order to subtract out the protein absorption band at 280 nm. [b] Kuhn anisotropy factor calculated from the CD intensity ($\Delta\epsilon$) in M^{-1} cm^{-1} and the absorption intensity (ϵ) in M^{-1} cm^{-1}. Expressed as $X \times 10^{-3}$.

small changes observed in the g values and hyperfine coupling constants [A_i ($i = x, y, z$) in Table 3] indicate that the T2 Cu site has been perturbed by the mutations at the D94 residue. In particular, the small g_z value shift observed in the T1DD94A mutant does not correlate with the energy shift observed for the $d_{xy} \rightarrow d_{x^2-y^2}$ transition (Table 4) and reflects a small covalency decrease at the T2 site.

The MCD spectra of T1D, T1DD94E, and T1DD94A are shown in Figure 2, and Table 4 presents the individual band energies of the MCD Gaussian fits. The four lowest energy bands (1−4) are the ligand field transitions and are assigned as $d_{xy} \rightarrow$, $d_{z^2} \rightarrow$, $d_{xz} \rightarrow$, and $d_{yz} \rightarrow d_{x^2-y^2}$ transitions in order of increasing energy (bands 1 to 4, respectively) (*7*). From Figure 2, changes can be observed in the ligand field region of the spectra of T1DD94E (Figure 2B) and T1DD94A (Figure 2C), as compared to T1D (Figure 2A). In particular, a small increase in the energies of the d_{xy}, d_{z^2}, and $d_{yz} \rightarrow d_{x^2-y^2}$ transitions (bands 1, 2, and 4, respectively) is observed, while the energy of the d_{xz} transition (band 3) decreases

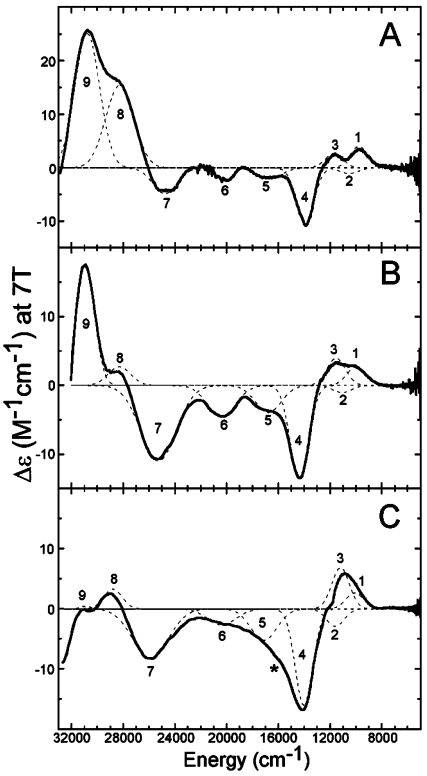

FIGURE 2: Low-temperature (5K) MCD spectra of Fet3p T1D (A), T1DD94E (B), and T1DD94A (C). Individual Gaussian bands with the parameters listed in Table 4 are shown in dotted lines.

(Table 4). The magnitude of the observed changes is most evident in the shape of the ligand field region of the T1DD94A spectrum (Figure 2C vs 2A). There is also an increase in intensity of some LF transitions (most notably, band 4). Ligand field transitions gain their intensity from mixing with ligand to metal CT transitions. Therefore, the increased intensity of some of the LF transitions in T1DD94E and T1DD94A correlates with the increased intensity of some CT bands (bands 5, 6, and 7 in Figure 2).

The next five bands (5−9) in the MCD spectrum of the T2 site (Figure 2) are ligand to metal CT transitions. Four of these bands correspond to His $\pi \rightarrow$ Cu $d_{x^2-y^2}$, two transitions (π_1 and π_2) from each of the two His ligands to the T2 site. The fifth CT band corresponds to an OH $\pi \rightarrow$ Cu $d_{x^2-y^2}$ (band 6), as assigned for the T2 site in T1Hg laccase (*7*). Overall, the CT transition energies do not change significantly in the D94 mutated proteins (Table 4); however, intensity changes are evident. In both, T1DD94E (Figure 2B) and T1DD94A (Figure 2C), bands 5, 6, and 7 increase in intensity, while bands 8 and 9 decrease compared to T1D (Figure 2A). The decreased intensity in band 9 is most pronounced in T1DD94A (Figure 2C). The observed intensity redistribution in the CT bands indicates that the strength of the interactions of the two histidines and the hydroxide ligand with the T2 Cu site in Fet3p have been perturbed in the D94 mutants.

(2.2) The T3 Site. In the absence of the T1 Cu site, the absorption and CD spectra of the T1-depleted proteins are dominated by the T3 Cu transitions (*19*, *33*). Figure 3 shows the absorption and CD spectra of T1D, T1DD94E ,and T1DD94A Fet3p. Simultaneous Gaussian fit of the absorption and CD spectra requires the presence of nine bands in the energy region from 5000 to 33000 cm^{-1}, as shown in Figure

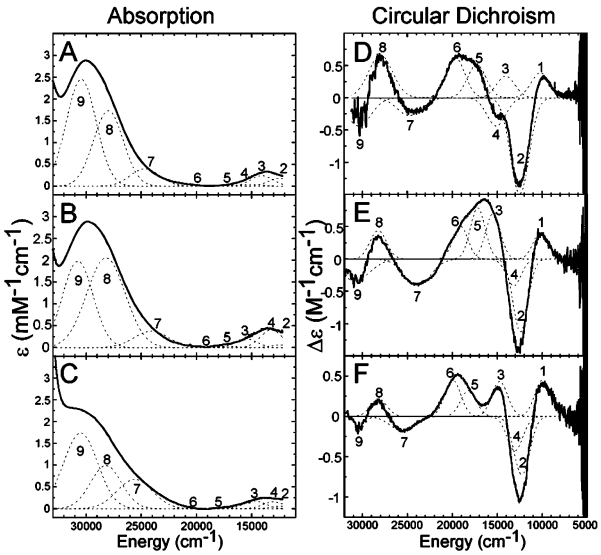

FIGURE 3: Room temperature difference absorption spectra (oxidized minus reduced) of Fet3p T1D (A), T1DD94E (B), and T1DD94A (C) and room temperature CD spectra of T1D (D), T1DD94E (E), and T1DD94A (F). Individual Gaussian bands with the parameters listed in Table 4 are shown in dotted lines.

3 and listed in Table 4. Based on their Kuhn anisotropy factors, i.e., the ratio of CD to absorption intensity ($\Delta\epsilon/\epsilon$ in Table 4, bottom), bands 1−6 are assigned as T3 Cu ligand field transitions in T1D Fet3p, while bands 7−9 are assigned as ligand to metal CT transitions (*18*).

In the absorption spectrum of T1D Fet3p (Figure 3A) there is an intense ($\epsilon \sim 3$ mM^{-1} cm^{-1})[3] transition at ~30300 cm^{-1}, which is resolved into two bands in the CD spectrum (Figure 3D, bands 8 and 9). These transitions are associated with the hydroxide bridge at the binuclear T3 Cu site and are assigned as two vector-coupled μ-OH → Cu^{2+} CT transitions, one for each of the two T3 coppers (*18*, *31*). The CD spectra show that the intensities of these transitions have changed in the D94E (Figure 3E) and D94A (Figure 3F) mutants; these changes are more pronounced in the D94A case. The shape of the broad absorption band at ~30300 cm^{-1} is also altered, most notably in the spectrum of T1DD94A (Figure 3C). These results indicate that the interaction of the OH bridge with the T3 Cu atoms has been perturbed upon mutation of the D94 residue.

The CD spectra of T1D (Figure 3D), T1DD94E (Figure 3E), and T1DD94A (Figure 3F) show differences in the ligand field region (bands 1−6). Relative to T1D the transition energies of bands 3 and 4 are shifted in T1DD94E (Table 4), which results in a notable change of shape in the 13000−20000 cm^{-1} region of its CD spectrum (Figure 3E). The changes in the LF region are even more evident in the T1DD94A case (Figure 3F), where the largest energy shifts were observed in bands 3, 4, and 5 (Table 4). The fact that more than four LF transitions can be resolved from the CD spectrum of Fet3p T1D indicates that the two T3 Cu ions are inequivalent, as observed in the T1Hg derivative of laccase (*19*). While LF bands 3, 4, and 5 are shifted in energy upon D94 mutation, LF bands 1, 2, and 6 did not significantly change, suggesting that one of the two Cu centers is more perturbed.

Finally, fluoride binding to the T1DD94A and T1DD94E mutants was studied by EPR. Both proteins bind fluoride

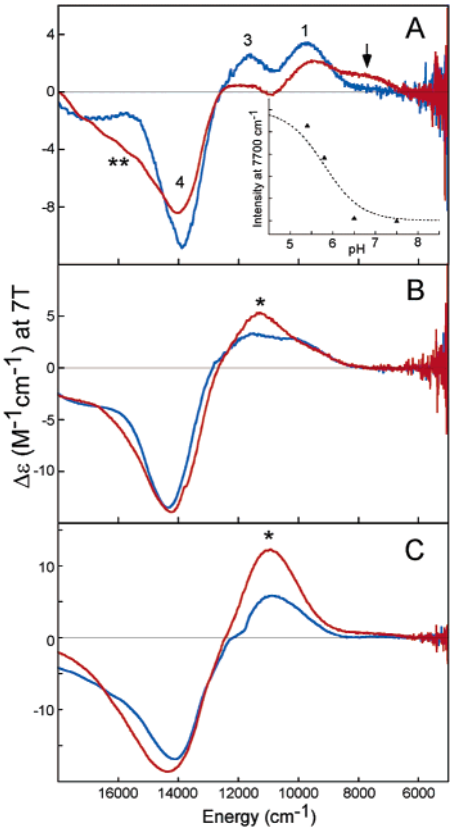

FIGURE 4: Low-temperature (5K) MCD spectra of Fet3p T1D (A), T1DD94E (B), and T1DD94A (C) at pD 7.5 (blue) and 5.8 (red). The inset in (A) shows the intensity at 7700 cm^{-1} as a function of pH (▲). The apparent change in the higher energy region of (A) (indicated by **) is due to a baseline shift.[6] The presence of a second species in the T1DD94E and T1DD94A spectra is indicated by an asterisk.[7]

with high affinity and form fluoride adducts with fluoride superhyperfine couplings similar to those observed in the T1D adduct (Figure S4, Supporting Information). High-affinity fluoride binding is a unique feature of the trinuclear cluster in the multicopper oxidases and is indicative of the integrity of the cluster. These results indicate that the oxidized T1DD94A and T1DD94E proteins contain a valid trinuclear cluster.

In summary, the Asp94 mutations to Glu and Ala have yielded proteins with stable trinuclear clusters that show some spectroscopic perturbations. The strength of the interactions of the T2 Cu site with its ligands, the OH bridge at the T3 site, and the ligand field at one of the T3 Cu centers have been most strongly perturbed. These effects are most pronounced in the D94A case where the carboxyl moiety has been eliminated.

(3) pH Effects on the Oxidized Trinuclear Cluster. The effect of pH on the spectroscopic features of the T2 site in Fet3p T1D was evaluated by EPR and MCD. The EPR spectra of T1D at pD 5.8 and 7.5 are identical (Figure S5, Supporting Information); however, the MCD spectra show changes in the ligand field region (Figure 4A), with a positive band at ~7700 cm^{-1} growing in at low pH (arrow in Figure 4A) with a pK_a <5.8 (Figure 4A, inset, ▲). Gaussian analysis shows an intensity redistribution in the LF transitions and a large shift of the $d_{xy} \rightarrow d_{x^2-y^2}$ transition (band 1) to lower energy (7700 cm^{-1}) at low pH. The CD spectrum of T1D does not change in the pH range studied (Figure S5,

Scheme 1: Hydrogen-Bonding Network between the D94 Residue and the Hydroxide Ligand at the T2 Cu

A) Resting oxidized at high pH: **B) Resting oxidized at low pH:**

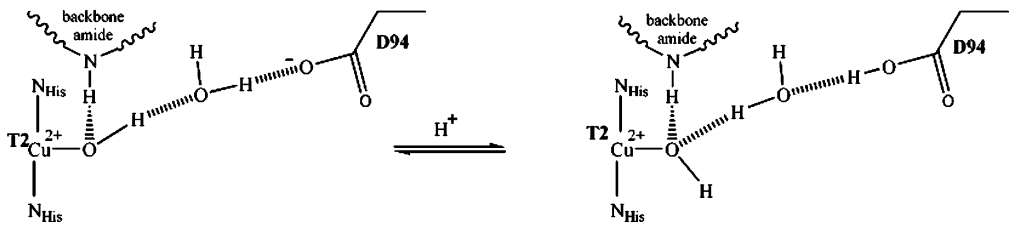

Supporting Information), indicating that the T3 site is not perturbed.

A similar pH effect has been observed in T1Hg laccase, where a positive T2 MCD band at ~7800 cm^{-1} grows in with a pK_a of 5.6 ± 0.3 (*7*). This pH effect is ascribed to the D72 residue in *Rhus vernicifera* laccase (equivalent to D94 in Fet3p and D73 in AO). In the crystal structure of AO (*11*), D73 is hydrogen bonded to a water molecule that in turn is hydrogen bonded to the OH ligand at the T2 site. Thus, protonation of this aspartate residue could change the orientation of the OH bond at the T2 Cu site, causing LF changes as observed by MCD (*7*).[5] Scheme 1 gives a model for the T2 OH ligand and its hydrogen bonds at high pH (structure A). A backbone amide that forms a conserved and strong hydrogen bond with the OH ligand is also included. When D94 is protonated at low pH (structure B), the hydrogen bonds to the water would rearrange, which in turn would change the orientation of the O−H bond at the T2 Cu.

In contrast to T1D, no pH effect is observed in the LF region of the MCD spectra of the T1DD94E and T1DD94A mutants (Figure 4B,C).[7] For the T1DD94A mutant, this is not suprising because the acidic side chain at this position has been eliminated. In the T1DD94E mutant, however, a carboxylic moiety is still present, and the lack of a pH effect indicates that either its pK_a has shifted to a lower value (<4.5) or the connectivity between the carboxylate and the hydroxide ligand at the T2 site has been eliminated. Since an *increase* of the pK_a value in the T1DD94E mutant is observed in other pH effects studied (section 4), it is reasonable to ascribe the lack of a pH effect in this mutant to the loss of connectivity with the T2 OH ligand.

(4) Oxygen Reactivity of the Trinuclear Cluster. The reaction of the three-electron reduced trinuclear cluster in Fet3p T1D with O_2 results in the formation of a peroxide-level intermediate with absorption features at 340 and 470 nm (*18*). The rate of formation of this intermediate was measured by stopped-flow absorption spectroscopy, as shown in Figure 5A. Single-wavelength data collected at 340 nm were fit to a single exponential to obtain the pseudo-first-order rate of formation (Figure 5A, inset). The rate of formation of the intermediate is pH dependent (Figure 5B, ■); the sigmoidal behavior is indicative of a single proton equilibrium with a pK_a of 6.3. No deuterium kinetic isotope effect is observed at low pH (data not shown). The rate of formation increases linearly with O_2 concentration, and no saturation behavior is observed (Figure S8, Supporting Information), suggesting that the rate-limiting step in the formation of the peroxide intermediate is O_2 binding. Previous studies of peroxide intermediate formation in T1Hg laccase showed a linear dependence of the rate on O_2 concentration (*34*), and no deuterium kinetic isotope effect, but exhibited no pH dependence (*17*). The spectroscopic

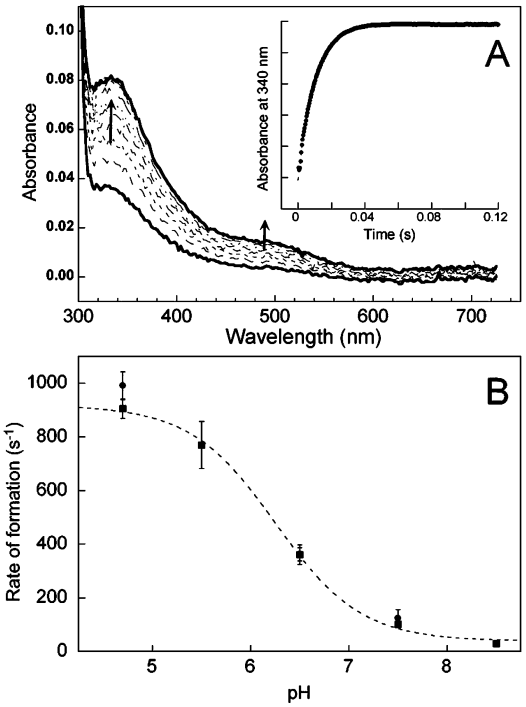

FIGURE 5: Formation of the peroxide intermediate in T1D at pH 7.5, as followed by stopped-flow absorption spectroscopy (A). The inset shows the absorbance increase at 340 nm; data were fit to a single exponential (dotted line) to obtain the first-order rate of formation. pH dependence of the rate of formation of the peroxide intermediate (B) in T1D (■) and T1DD94E (●). The T1D data were fit with an expression derived from a protonation equilibrium model: $k_{obs} = (k_2[H^+] + k_1K_a)/(K_a + [H^+])$, where k_1 is the rate at high pH, k_2 is the rate at low pH, and K_a is the equilibrium constant of the protonatable group.

[5] The largest shift is observed in the $d_{xy} \rightarrow d_{x^2-y^2}$ transition, yet no g_z or A_z change is observed, indicating concomitant small covalency changes at low pH. The ligand field and covalency changes occur mostly at the d_{xy} orbital, which has a π interaction with the O p_y and a pseudo-σ interaction with the O p_z orbital and is the most affected by a change in orientation of the O−H bond.

[6] The data shown in Figure 4A were collected with a J200 instrument that has best resolution in the near-IR region but some baseline shifts at higher energy (above 14000 cm^{-1}). This baseline shift problem is more pronounced in the T1D Fet3p samples at low pH, which tend to yield lower quality glasses. Better data on the higher energy region have been collected with a J810 instrument on comparable samples (Figure S6, Supporting Information), showing that the apparent changes in the 16000 cm^{-1} region are due to a baseline effect.

[7] An intensity increase is observed around 11000 cm^{-1} in both T1DD94E and T1DD94A at low pH. However, this change is not reversible with pH (Figure S7A, Supporting Information) and is ascribed to the presence of the denatured site that could not be completely removed by chelating resin. The amount of the second species is almost negligible in T1DD94E (Figure S7B) and is most evident in T1DD94A by EPR (Figure S7C).

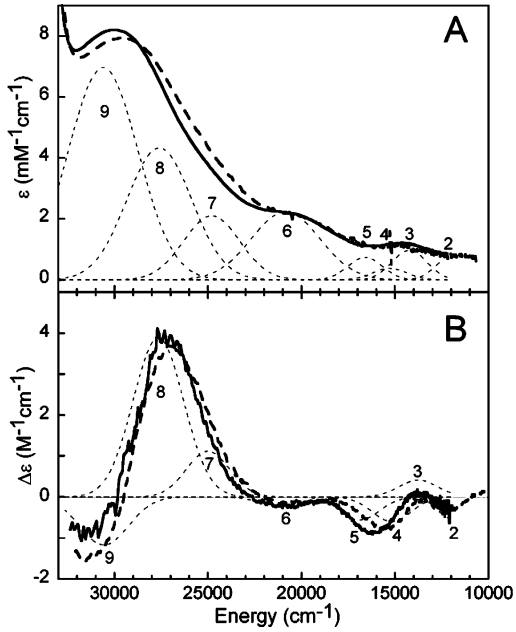

FIGURE 6: Room temperature absorption (A) and CD (B) spectra of the peroxide intermediates of Fet3p T1D (solid lines) and T1DD94E (dashed lines). Individual Gaussian bands for the T1D intermediate are shown in dotted lines; bands 2−5 have been assigned as T3 Cu LF transitions, while bands 6−9 correspond to peroxide π^*_v and $\pi^*_\sigma \rightarrow$ T3 Cu^{2+} CT transitions, as previously reported (*16*, *18*, *19*).

similarity of the peroxide intermediates in T1Hg laccase (*17*) and T1D Fet3p (*18*) and their comparable rates of formation (which implies comparable driving forces for this reaction) indicate that a proton can participate in but is not required for the formation of the peroxide intermediate. Moreover, the pK_a associated with the formation of the peroxide intermediate in Fet3p argues against the involvement of a carboxylic residue in this reaction.

The analogous reaction of reduced T1DD94E with O_2 generates a transient species with an absorption spectrum similar to that of the T1D intermediate (Figure 6A), indicating that a peroxide intermediate is formed in T1DD94E. Consistent with this assignment, no EPR signal and no LF transitions were observed in the MCD spectrum of this species (Figure S9, Supporting Information), demonstrating that the T2 Cu site is reduced and the T3 coppers are strongly antiferromagnetically coupled through a bridging ligand. The rates of formation of the T1DD94E peroxide intermediate (Figure 5B, ●) are identical to those obtained for T1D, indicating that the D94E mutation does not affect the initial reaction of the trinuclear cluster with O_2. A comparison of the absorption and CD spectra of the T1D and T1DD94E peroxide intermediates is shown in Figure 6. The overall shape and intensities of the CT bands are comparable, indicating that the peroxide binds in a similar mode. However, a small shift to lower energy is evident in the T1DD94E intermediate spectra (Figure 6, dashed lines) relative to T1D (Figure 6, solid lines), and all bands shift by the same amount (~400 cm^{-1}). Since the d_{z^2} is the acceptor orbital of these transitions, this implies that the d_{z^2} ground state at the T3 Cu centers must be at lower energy (i.e., less destabilized) in the T1DD94E intermediate. This observation is consistent with the small perturbations to the electronic structure of the T3 site caused by the D94E mutation characterized in section 2.2.

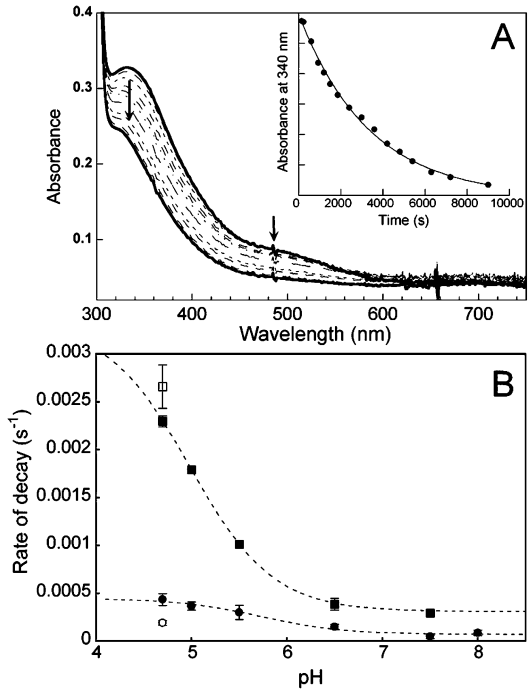

FIGURE 7: Decay of the peroxide intermediate in T1DD94E, as followed by absorption (A). The inset shows the absorbance decay at 340 nm at pH 5.5; data were fit to a single exponential (line) to obtain the first-order rate of decay. pH dependence of the rate of decay of the peroxide intermediate (B) in T1D (■) and T1DD94E (●). The data were fit with an expression derived from a protonation equilibrium model: $k_{obs} = (k_2[H^+] + k_1K_a)/(K_a + [H^+])$, where k_1 is the rate at high pH, k_2 is the rate at low pH, and K_a is the equilibrium constant of the protonatable group (*17*). pH data for T1D were taken from ref *18*. Data collected in deuterated buffer are shown with open symbols.

In contrast to T1D and T1DD94E, reduced T1DD94A protein does not react with O_2, and no peroxide intermediate is observed (Figure S10A). Similarly, reduced D94A protein does not react with O_2, no native intermediate is present, and only a slow reoxidation of the T1 site is observed (Figure S10B), indicative of outer-sphere electron transfer. These results demonstrate that the D94A mutation has eliminated the oxygen reactivity of the trinuclear cluster. Spectroscopic studies of the T1D proteins in section 2 show that the D94A mutation causes larger structural changes at the T2 and T3 Cu sites than the D94E mutation. This larger structural perturbation caused by the D94A mutation has rendered the trinuclear cluster unreactive toward O_2.

(5) Decay of the Peroxide Intermediate. The decay of the peroxide intermediate in T1D Fet3p has been studied by monitoring the loss in absorption intensity of the peroxide CT bands at 340 and 480 nm. The intermediate decays slowly to resting oxidized T1D Fet3p, and the rate of decay is pH dependent with a pK_a of 5.0 ± 0.2 (included for reference in Figure 7B, ■) (*18*). The sigmoidal behavior of the pH dependence of the peroxide intermediate decay rate has been ascribed to a protonation equilibrium model, where intermediate decay is accelerated upon protonation of a nearby carboxylate residue at low pH (*17*, *18*).

The results from parallel studies on the decay of the peroxide intermediate of T1DD94E are given in Figure 7. The absorption intensity decay (Figure 7A) can be fit to a single exponential to extract a first-order rate constant. For T1DD94E, the rate of decay is also pH dependent (Figure

7B, ●), but with a different pK_a (5.7 ± 0.2) and a much smaller rate enhancement at low pH, indicating that the protonation of the carboxylate residue is not as effective in enhancing the rate as it is in the T1D case.

The kinetic solvent isotope effect (KSIE) on the rate of decay of the peroxide intermediate was measured at pH/pD 4.7 to obtain information about the transition state involved in proton transfer. For the T1D intermediate, a marginally inverse KSIE is observed ($k_H/k_D = 0.86 \pm 0.10$; Figure 7B, □). A similar inverse KSIE has been observed for the decay of the peroxide intermediate in T1Hg laccase at low pH (*17*), suggesting that the proton of interest is bound more tightly in the transition state than in the reactant state (*35*). However, for the T1DD94E intermediate a normal and larger KSIE is observed ($k_H/k_D = 2.29 \pm 0.19$; Figure 7B, ○). The facts that the rate enhancement with pH is much smaller and that the KSIE is no longer inverse in T1DD94E indicate that the nature of the transition state in this mutant has changed.

In summary, the trinuclear cluster in the T1DD94E mutant is capable of reaction with oxygen and forms a peroxide intermediate that is structurally comparable to that of T1D Fet3p. However, kinetic studies on the intermediate decay indicate that the mechanism by which a proton assists the decay of the peroxide intermediate in T1DD94E is different from that of the T1D protein.

DISCUSSION

The mutations of the Asp94 residue to Glu and Ala generate stable trinuclear Cu clusters in Fet3p. Spectroscopic studies have shown that these mutations perturb the geometric and electronic structure of the trinuclear cluster. In particular, the strength of the interactions of the T2 Cu with its two histidines and one hydroxide ligand, the nature of the OH bridge at the T3 site, and the ligand field at one of the T3 Cu centers are affected. In the crystal structure of AO (*11*), the D73 residue (equivalent to D94 in Fet3p) interacts with the hydroxide ligand of the T2 site through hydrogen bonds (Figure 8). The carboxylic moiety of D73 is hydrogen bonded to a water molecule which, in turn, is hydrogen bonded to the T2 hydroxide ligand. Both of the D94 mutations studied above would perturb this hydrogen-bonding network and, therefore, affect the interaction of the hydroxide ligand with the T2 Cu. The mutation of D94 to a longer glutamate side chain would change the spatial arrangement of the water molecule, while the elimination of the carboxylic moiety in the D94A mutant would abolish the connectivity of this residue with the OH ligand of the T2 site. The carboxylic moiety of D73 in AO (D94 in Fet3p) is also hydrogen bonded to the noncoordinating Nδ of His450 (H418 in Fet3p), which is the axial histidine ligand to the T3 Cu$_\beta$ atom (Figure 8). A comparable scenario is present in the crystal structures of other multicopper oxidases, including fungal laccases, *Bacillus subtilis* CotA, and *Escherichia coli* CueO (*36*−*40*), and diffraction data for Fet3p collected to 2.8 Å indicate that there is a similar arrangement for the D94 residue in this protein (*41*).[8] Mutation of D94 to a longer glutamate residue could change the orientation of the axial histidine ligand at T3 Cu$_\beta$. Similarly, elimination of the carboxyl group in the D94A mutant would abolish any constraint that the D94 residue may place on the orientation of the histidine ring. Ligand field calculations

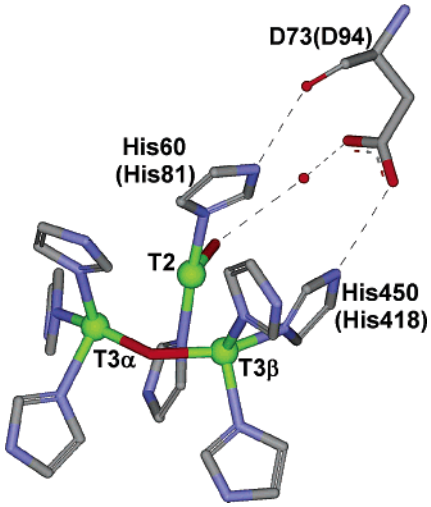

FIGURE 8: Hydrogen bond connectivity of the D73 residue (D94 in Fet3p) with the trinuclear Cu cluster. This figure was generated from the crystal structure of AO (PDB accession number 1AZO) (*11*). Sequence numbers in parentheses correspond to Fet3p, and Cu atoms are shown in green. T3 Cu$_\alpha$ (also referred to as Cu3) corresponds to the Cu atom ligated to His62, His104, and His508, while the T3 Cu$_\beta$ atom (also referred to as Cu2) is ligated to His106, His450, and His506.

show that the T3 Cu has a half-filled d_{z^2} ground state and approximate trigonal bipyramidal geometry with an open coordination position in the equatorial plane (*19*). The dominant bonding interactions that determine the orientation of the T3 Cu$_\beta$ d_{z^2} orbital involve the axial His418 and the OH bridge. Therefore, perturbations of the orientation of the axial His418 ligand would affect the ligand field at the T3 Cu$_\beta$ atom and its interaction with the bridging hydroxide, as observed in T1DD94E and T1DD94A.

A third connectivity between the D94 residue and the trinuclear cluster is given by a hydrogen bond between the D94 backbone carbonyl and the noncoordinating Nδ of His81 (His60 in AO), one of the histidine ligands of the T2 Cu site (Figure 8). Since the D94 mutations disturb the hydrogen-bonding network of the carboxyl moiety, they are likely to affect the orientation of the backbone as well, disrupting the hydrogen bond connectivity between the D94 backbone carbonyl and His81. This in turn would alter the bonding interaction of His81 with the T2 Cu, resulting in intensity redistribution of the His $\pi \rightarrow$ Cu $d_{x^2-y^2}$ CT bands, as observed by MCD (section 2).

Therefore, the D94 mutations perturb the electronic structure of the T2 and T3 Cu sites in a way that is consistent with the hydrogen bond connectivity of D94 with the cluster (Figure 8). These hydrogen bonds are highly conserved in the multicopper oxidases[8] and are part of a large hydrogen-bonding network around the trinuclear Cu cluster that

[8] The crystal structures of *E. coli* CueO (1.4 Å resolution, ref *37*), *B. subtilis* CotA (1.7 Å resolution, ref *38*), and *Trametes versicolor* laccase (1.9 Å resolution, ref *40*) show hydrogen-bonding networks identical to that in Figure 8. The crystal structures of *Melanocarpus albomyces* laccase (2.4 Å resolution, ref *36*), *T. versicolor* laccase (at 2.4 Å resolution, ref *39*), and Fet3p (2.8 Å resolution, ref *41*) show the D94 residue in a comparable position, where the two hydrogen bond connectivities to the T2 His and to one of the T3 axial His are conserved; however, the hydrogen bond connectivity between the D94 carboxylate and the T2 hydroxide ligand is not resolved, probably due to the lower resolution of the structures.

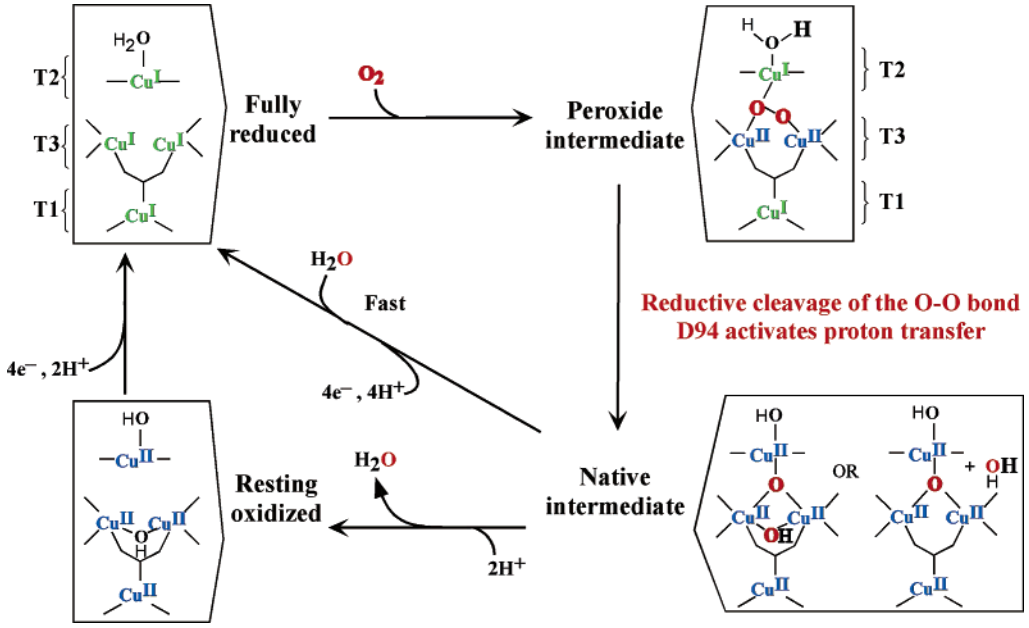

FIGURE 9: Proposed mechanism for the multicopper oxidases (adapted from ref *12*).

Scheme 2: Hydrogen-Bonding Network between the D94 Residue and the Water-Derived Ligand at the T2 Cu in the Peroxide Intermediate

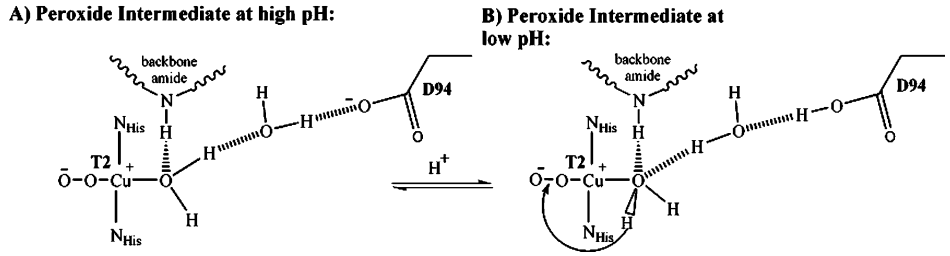

contributes to its stability and oxygen reactivity, as shown previously in the study of several mutations around the trinuclear Cu cluster in Fet3p (*18*). While the D94E mutation does not affect the initial reaction of the cluster with O_2, the larger structural changes caused by the D94A mutation render the trinuclear cluster unreactive toward O_2. These results establish a structural role for the D94 and its hydrogen bond connectivity that is relevant for the oxygen reactivity of the trinuclear cluster.

While the D94E mutation still allows for oxygen reactivity and peroxide intermediate formation, it eliminates the pH effect observed in the resting T2 Cu site. Thus, the hydrogen bond connectivity between the D94 carboxyl group and the T2 OH ligand in T1D (Scheme 1) is disrupted in the D94E mutant. The D94E mutation also completely changes the properties of the decay of the peroxide intermediate and its pH dependence; it shows slower decay rates, different pK_a (5.8 ± 0.2), significantly smaller rate enhancement, and strikingly different KSIE at low pH. These results indicate that the mechanism of rate enhancement at low pH has been perturbed with the D94E mutation. Thus, the D94E mutant demonstrates that the D94 residue is responsible for both the pH effect on the resting T2 Cu site and the pH dependence and rate enhancement at low pH of the decay of the peroxide intermediate in T1D Fet3p. Consistent with this assignment, for T1D the pK_a associated with the decay of the peroxide intermediate (5.0 ± 0.2) falls within the range estimated for the pH effect on the resting T2 Cu by MCD (<5.8).

Figure 9 shows the proposed catalytic mechanism for the multicopper oxidases. The reduction of O_2 to water involves two $2e^-$ steps (*12*). When the enzyme is deprived of 1 electron equivalent (as in the T1D derivatives), the decay of the peroxide intermediate becomes a slow one-electron process. It has been shown that the peroxide intermediate decays to the resting oxidized protein through a native intermediate-like species (*16*). Therefore, although this process is too slow to be catalytically relevant, it provides insight into the reductive cleavage of the O−O bond.

In the peroxide intermediate, the reduced T2 Cu and the oxidized T3 coppers are bridged by the peroxide (Figure 9) (*16*−*19*). Upon decay, the T2 site is oxidized and an electron is transferred to the peroxide species for O−O bond cleavage. Detailed spectroscopic studies on the resting oxidized form of the T2 Cu site have shown that the water-derived ligand at the T2 Cu is a hydroxide over the pH range of 4.7−10.0 (*7*). Thus, the water ligand at the T2 Cu^+ in the peroxide intermediate (Figure 9) must get deprotonated upon oxidation of the T2 site. Our pH studies on the T2 site have also shown that protonation of D94 affects the orientation of the OH bond (Scheme 1), and a similar connectivity between the Cu^+-bound water and the D94 residue reasonably exists in the peroxide intermediate (Scheme 2). Protonation of D94 would then cause both a perturbation of the water ligand at the T2 Cu and an acceleration of the rate of decay of the peroxide intermediate, suggesting that these two events are associated. Thus, deprotonation of the T2 water may be involved in the transition state of this reaction.

The observed inverse KSIE at low pH in the decay of the peroxide intermediate is consistent with the involvement of a metal-bound water in the transition state (*17*). If this proton is transferred to the Cu-bound peroxide, the O−H bond being formed in the transition state would be stronger than in the Cu-bound water of the reactant state. Transfer of an electron from the reduced T2 Cu to the peroxide would increase the positive charge of the Cu and its inductive effect, lowering the pK_a of the Cu-bound water and facilitating the proton transfer from the T2 Cu-bound water to the peroxide (as indicated by the arrow in Scheme 2, structure B). Protonation of the peroxide decreases the energy of the peroxide σ^* orbital (*42*), lowering the barrier for the O−O bond cleavage.[9]

Thus, the proton that assists the reductive cleavage of the O−O bond in Figure 9 could be provided by the T2 Cu^+-bound water in the peroxide intermediate. The role of the protonation of D94 would then be to activate this Cu-bound water to participate in the transition state, lowering the barrier for O−O cleavage and accelerating the reaction. As illustrated in Scheme 2, at low pH (structure B), the Cu^+-bound water could form two hydrogen bonds, one with the backbone amide and one with the nearby water molecule. These two hydrogen bonds would help to stabilize the formation of the T2 Cu^{2+}-OH species along the reaction coordinate. At high pH (structure A), there would be only one hydrogen bond to the oxygen (with the backbone amide), and a proton from the T2 Cu-bound water would be engaged in a hydrogen bond with the nearby water molecule. This configuration would stabilize the water over the hydroxo species, preventing this proton from participating in the transition state of the reaction. This is consistent with the lack of a KSIE in the decay of the peroxide intermediate at high pH.

In summary, the study of mutations at the D94 residue has provided further insight into the role of protons in the O_2 reactivity of Fet3p. While the lack of O_2 reactivity of the D94A mutant suggests that the D94 residue and its hydrogen bond connectivity play a structural role that is relevant for reactivity, the D94E mutation confirms the involvement of D94 in the decay of the peroxide intermediate. In this reaction, the conjugate acid form of the D94 residue appears to activate a proton transfer from the T2 Cu^+-bound water to assist in the reductive cleavage of the O−O bond. These conclusions can be extended to the $2e^-$ cleavage in the native enzyme. The use of T1D derivatives has slowed down a key step in the catalytic mechanism, which is otherwise very fast in the native enzyme, and has provided important insight into proton involvement in the reductive cleavage of the O−O bond.

ACKNOWLEDGMENT

We thank Prof. P. John Hart at The University of Texas, San Antonio, for sharing preliminary crystallographic results on Fet3p and Dr. Brenda Valderrama and co-workers at Insituto de Biotecnología, Universidad Nacional Autónoma de México, for sharing sequence alignments of fungal laccases.

SUPPORTING INFORMATION AVAILABLE

Oxidation of the holo proteins followed by absorption and EPR; absorption, CD, MCD, and EPR spectra of the holo proteins; EPR comparison of the fluoride adducts of the T1D mutants; EPR and CD spectra of T1D at high and low pH; MCD spectra of T1D at pD 5.8 collected on different instruments; MCD spectra of T1DD94E at different pHs, EPR spectra of T1DD94E and T1DD94A at high and low pH; rates of formation of the peroxide intermediate in T1D as a function of oxygen concentration; EPR and MCD spectra of the T1DD94E peroxide intermediate; and absorption spectra of reduced D94A mutants and their exposure to O_2. This material is available free of charge via the Internet at http://pubs.acs.org.

REFERENCES

1. Solomon, E. I., Sundaram, U. M., and Machonkin, T. E. (1996) Multicopper oxidases and oxygenases, *Chem. Rev. 96*, 2563−2605.
2. Askwith, C., Eide, D., VanHo, A., Bernard, P. S., Li, L., Davis-Kaplan, S., Sipe, D. M., and Kaplan, J. (1994) The FET3 gene of *S. cerevisiae* encodes a multicopper oxidase required for ferrous iron uptake, *Cell 76*, 403−410.
3. de Silva, D., Askwith, C. C., Eide, D., and Kaplan, J. (1995) The FET3 gene product required for high affinity iron transport in yeast is a cell surface ferroxidase, *J. Biol. Chem. 270*, 1098−1101.
4. Hassett, R. F., Yuan, D. S., and Kosman, D. J. (1998) Spectral and kinetic properties of the Fet3 protein from *Saccharomyces cerevisiae*, a multinuclear copper ferroxidase enzyme, *J. Biol. Chem. 273*, 23274−23282.
5. Stearman, R., Yuan, D. S., Yamaguchi-Iwai, Y., Klausner, R. D., and Dancis, A. (1996) A permease-oxidase complex involved in high-affinity iron uptake in yeast, *Science 271*, 1552−1557.
6. Askwith, C., and Kaplan, J. (1998) Iron and copper transport in yeast and its relevance to human disease, *Trends Biochem. Sci. 23*, 135−138.
7. Quintanar, L., Yoon, J., Aznar, C., Palmer, A. E., Andersson, K., Britt, D., and Solomon, E. I. (2004) Spectroscopic and electronic structure studies of T1 mercury laccase: the nature of the trinuclear Cu cluster and its coordination unsaturation, *J. Am. Chem. Soc.* (submitted for publication).
8. Allendorf, M. D., Spira, D. J., and Solomon, E. I. (1985) Low temperature MCD studies of native laccase: spectroscopic evidence for exogenous ligand bridging at a trinuclear copper active site, *Proc. Natl. Acad. Sci. U.S.A. 82*, 3063.
9. Spira-Solomon, D. J., Allendorf, M. D., and Solomon, E. I. (1986) Low-temperature magnetic circular dichroism studies of native laccase: confirmation of a trinuclear copper active site, *J. Am. Chem. Soc. 108*, 5318.
10. Cole, J. L., Tan, G. O., Yang, E. K., Hodgson, K. O., and Solomon, E. I. (1990) Reactivity of the laccase trinuclear copper active site with dioxygen: an X-ray absorption edge study, *J. Am. Chem. Soc. 112*, 2243−2249.
11. Messerschmidt, A., Ladenstein, R., Huber, R., Bolognesi, M., Avigliano, L., Petruzzelli, R., Rossi, A., and Finazzi-Agro, A. (1992) Refined crystal structure of ascorbate oxidase at 1.9 Å resolution, *J. Mol. Biol. 224*, 179−205.
12. Solomon, E. I., Chen, P., Metz, M., Lee, S.-K., and Palmer, A. E. (2001) Oxygen binding, activation, and reduction to water by copper proteins, *Angew. Chem., Int. Ed. 40*, 4570−4590.
13. Andréasson, L.-E., and Reinhammar, B. (1976) Kinetic studies of *Rhus vernicifera* laccase. role of the metal centers in electron transfer, *Biochim. Biophys. Acta 445*, 579−597.
14. Andréasson, L.-E., Brändén, R., and Reinhammar, B. (1976) Kinetic studies of *Rhus vernicifera* laccase: evidence for multielectron transfer and an oxygen intermediate in the reoxidation reaction, *Biochim. Biophys. Acta 438*, 370−379.

[9] The activation energies for the decay of the peroxide intermediate in T1Hg laccase at high and low pH have been determined to be the same within experimental error. The 10× rate enhancement for the decay of the peroxide intermediate at low pH amounts to a 1.4 kcal/mol difference in activation energy, which is within the error of the data.

15. Lee, S. K., George, S. D., Antholine, W. E., Hedman, B., Hodgson, K. O., and Solomon, E. I. (2002) Nature of the intermediate formed in the reduction of O_2 to H_2O at the trinuclear copper cluster active site in native laccase, *J. Am. Chem. Soc. 124*, 6180−6193.
16. Shin, W., Sundaram, U. M., Cole, J. L., Zhang, H. H., Hedman, B., Hodgson, K. O., and Solomon, E. I. (1996) Chemical and spectroscopic definition of the peroxide-level intermediate in the multicopper oxidases: relevance to the catalytic mechanism of dioxygen reduction to water, *J. Am. Chem. Soc. 118*, 3202−3215.
17. Palmer, A. E., Lee, S.-K., and Solomon, E. I. (2001) Decay of the peroxide intermediate in laccase: reductive cleavage of the O−O bond, *J. Am. Chem. Soc. 123*, 6591−6599.
18. Palmer, A. E., Quintanar, L., Severance, S., Wang, T.-P., Kosman, D. J., and Solomon, E. I. (2002) Spectroscopic characterization and O_2 reactivity of the trinuclear Cu cluster of mutants of the multicopper oxidase Fet3p, *Biochemistry 41*, 6438−6448.
19. Sundaram, U. M., Zhang, H. H., Hedman, B., Hodgson, K. O., and Solomon, E. I. (1997) Spectroscopic investigation of peroxide binding to the trinuclear copper cluster site in laccase: correlation with the peroxy-level intermediate and relevance to catalysis, *J. Am. Chem. Soc. 119*, 12525−12540.
20. Messerschmidt, A., Rossi, A., Ladenstein, R., Huber, R., Bolognesi, M., Guiseppina, G., Marchesini, A., Petruzzelli, R., and Finazzi-Agro, A. (1989) X-ray crystal structure of the blue oxidase ascorbate oxidase from zucchini. Analysis of the polypeptide fold and model of the copper sites and ligands, *J. Mol. Biol. 206*, 513−529.
21. Nitta, K., Kataoka, K., and Sakurai, T. (2002) Primary structure of a Japanese lacquer tree laccase as a prototype enzyme of multicopper oxidases, *J. Inorg. Biochem. 91*, 125−131.
22. Ducros, V., Brzozowski, A. M., Wilson, K. S., Brown, S. H., Østergaard, P., Schneider, P., Yaver, D. S., Pedersen, A. H., and Davis, G. J. (1998) Crystal structure of the type-2 Cu depleted laccase from *Coprinus cinereus* at 2.2 Å resolution, *Nat. Struct. Biol. 5*, 310−316.
23. Jonsson, L., Sjostrom, K., Haggstrom, I., and Nyman, P. O. (1995) Characterization of a laccase gene from the white-rot fungus *Trametes versicolor* and structural features of basidiomycete laccases, *Biochim. Biophys. Acta 1251*, 210−215.
24. Silva, D. M. D., Askwith, C., Eide, D., and Kaplan, J. (1995) The FET3 gene product required for high affinity iron transport in yeast is a cell surface ferroxidase, *J. Biol. Chem. 270*, 1098−1101.
25. Valderrama, B., Olivier, P., Medrano-Soto, A., and Vazquez-Duhalt, R. (2003) Evolutionary and structural diversity of fungal laccases, *Antonie van Leeuwenhoek 84*, 289−299.
26. Yaver, D. S., Xu, F., Golightly, E. J., Brown, K. M., Brown, S. H., Rey, M. W., Schneider, P., Halkier, T., Mondorf, K., and Dalboge, H. (1996) Purification, characterization, molecular cloning, and expression of two laccase genes from the white rot basidiomycete *Trametes villosa*, *Appl. Environ. Microbiol. 62*, 834−841.
27. Wang, T.-P., Quintanar, L., Severance, S., Solomon, E. I., and Kosman, D. J. (2003) Targeted suppression of the ferroxidase and iron trafficking activities of the multicopper oxidase Fet3p from *Saccharomyces cerevisiae*, *J. Biol. Inorg. Chem. 8*, 611−620.
28. Bradford, M. M. (1976) A rapid and sensitive method for the quantitation of microgram quantities of protein utilizing the principle of protein-dye binding, *Anal. Biochem. 72*, 248−254.
29. Felsenfeld, G. (1960) The determination of cuprous ion in copper proteins, *Arch. Biochem. Biophys. 87*, 247−251.
30. Carithers, R. P., and Palmer, G. (1981) Characterization of the potentiometric behavior of soluble cytochrome-oxidase by magnetic circular dichroism: evidence in support of heme-heme interaction, *J. Biol. Chem. 256*, 7967−7976.
31. Machonkin, T. E., Quintanar, L., Palmer, A. E., Hassett, R., Severance, S., Kosman, D. J., and Solomon, E. I. (2001) Spectroscopy and reactivity of the type 1 copper site in Fet3p from *Saccharomyces cerevisiae*: correlation of structure with reactivity in the multicopper oxidases, *J. Am. Chem. Soc. 123*, 5507−5517.
32. Kosman, D. J., Hassett, R., Yuan, D. S., and McCracken, J. (1998) Spectroscopic characterization of the Cu(II) Sites in the Fet3 protein, the multinuclear copper oxidase from yeast required for high-affinity iron uptake, *J. Am. Chem. Soc. 120*, 4037−4038.
33. Cole, J. L., Clark, P. A., and Solomon, E. I. (1990) Spectroscopic and chemical studies of the laccase trinuclear copper active site: geometric and electronic structure, *J. Am. Chem. Soc. 112*, 9534−9548.
34. Cole, J. L., Ballou, D. P., and Solomon, E. I. (1991) Spectroscopic characterization of the peroxide intermediate in the reduction of dioxygen catalyzed by the multicopper oxidases, *J. Am. Chem. Soc. 113*, 8544−8546.
35. Klinman, J. P. (1978) Kinetic isotope effects in enzymology, *Adv. Enzymol. 46*, 415−494.
36. Hakulinen, N., Kiiskinen, L., Kruus, K., Saloheimo, M., Paananen, A., Koivula, A., and Rouvinen, J. (2002) Crystal structure of a laccase from *Melanocarpus albomyces* with an intact trinuclear copper site, *Nat. Struct. Biol. 9*, 601−605.
37. Roberts, S., Weichsel, A., Grass, G., Thakali, K., Hazzard, J., Tollin, G., Rensing, C., and Montfort, W. (2002) Crystal structure and electron-transfer kinetics of CueO, a multicopper oxidase required for copper homeostasis in *Escherichia coli*, *Proc. Natl. Acad. Sci. U.S.A. 99*, 2766−2771.
38. Enguita, F., Martins, L., Henriques, A., and Carrondo, M. (2003) Crystal structure of a bacterial endospore coat component−a laccase with enhanced thermostability properties, *J. Biol. Chem. 278*, 19416−19425.
39. Bertrand, T., Jolivalt, C., Briozzo, P., Caminade, E., Joly, N., Madzak, C., and Mougin, C. (2002) Crystal structure of a four-copper laccase complexed with an arylamine: insights into substrate recognition and correlation with kinetics, *Biochemistry 41*, 7325−7333.
40. Piontek, K., Antorini, M., and Choinowski, T. (2002) Crystal structure of a laccase from the fungus *Trametes versicolor* at 1.90-Å resolution containing a full complement of coppers, *J. Biol. Chem. 277*, 37663−37669.
41. Taylor, A. B., Stoj, C., Kosman, D. J., and Hart, P. J. (2005) unpublished results.
42. Root, D. E., Mahroof-Tahir, M., Karlin, K. D., and Solomon, E. I. (1998) Effect of protonation on peroxo-copper bonding: spectroscopic and electronic structure study of $[Cu_2((UN\text{-}O\text{-})(OOH)]^{2+}$, *Inorg. Chem. 37*, 4838−4848.

BI047379C